http://dx.doi.org/10.1016/j.ijfatigue.2008.07.018

International Journal of Fatigue
Volume 31, Issue 3, March 2009, Pages 425-432

Prediction of fatigue crack growth and residual life using an exponential model: Part II (mode-I overload induced retardation)

J.R. Mohanty[a], B.B. Verma[a] and P.K. Ray[b],

[a]Department of Metallurgical and Materials Engineering, National Institute of Technology, Rourkela 769 008, India

[b]Department of Mechanical Engineering, National Institute of Technology, Rourkela 769 008, India

Prediction of fatigue crack growth and residual life using an exponential model: Part II (mode-I overload induced retardation)

J.R. Mohanty [a], B.B. Verma [a], P.K. Ray [b,*]

[a] Department of Metallurgical and Materials Engineering, National Institute of Technology, Rourkela 769 008, India
[b] Department of Mechanical Engineering, National Institute of Technology, Rourkela 769 008, India

A B S T R A C T

Almost all load bearing components usually experience variable amplitude loading (VAL) rather than constant amplitude loading (CAL) during their service lives. A single overload cycle introduced in a constant amplitude fatigue loading retards fatigue crack growth and increases residual fatigue life. Although many models have been proposed on this subject, but life prediction under these complex situations is still under constant improvement. The present study aims at evaluating retardation in fatigue life due to application of a single tensile overload spike by adopting an exponential model. The proposed model calculates not only parameters related with overload induced retardation in fatigue crack growth, but also residual life in case of 7020-T7 and 2024-T3 aluminum alloys with reasonable accuracy without integration of rate equation. The model also covers stage-II and stage-III of post-overload period.

1. Introduction

Fatigue performance of structures is greatly affected by the presence of stress raisers such as fastener holes, manufacturing errors, corrosion pits, and maintenance damage which serve as nucleation sites for fatigue cracking. During service, sub-critical cracks nucleate from these sites and grow till catastrophic failure (unstable crack growth) takes place when the crack length reaches a critical dimension. From economic point of view a costly component cannot be retired from service simply on detecting a fatigue crack. Hence, reliable estimation of fatigue crack propagation and residual life prediction are essential so that the component can be timely serviced or replaced. Many load bearing structural components experience variable amplitude loading during the length of service. The assessment of fatigue life of structural components subjected to these transient effects becomes complicated due to lack of reliable methodology. Variable amplitude loading involves load interaction effects and significantly affects the fatigue crack growth and consequently the fatigue life leading to either retardation (an overload tensile in nature) or acceleration (an under load compressive in nature) or reduction in retardation (an overload followed by an under load).

A great deal of scientific and academic investigation has been focused in the literature on fatigue crack growth retardation resulting from single and multiple overloads. The demand for longer service life and the acceptance of pre-existing flaws (damage-tolerant design) have encouraged the aircraft industry to enhance the fatigue life by giving controlled yielding (or overload) on the material ahead of crack tip by introducing compressive residual stress [1–6]. However the micro-mechanisms governing the retardation phenomena are still not well understood [7–12]. Some researchers attributed the primary cause for overload induced retardation to be residual plastic zone ahead of the crack tip created by the overload. Other causes may be crack tip blunting, crack branching, plasticity induced closure and roughness induced closure. In recent years Sadananda and Vasudevan [7] reported that closure occurring behind the crack tip has limited effect on the damage process that takes place in front of the crack. Later on several research activities were conducted [8–13] and it is concluded that fatigue crack growth not only depends on single crack driving forces ΔK but also on maximum stress intensity factor K_{max}. This leads to a new approach called two-parameter crack driving force or the unified approach.

A number of empirical models have been developed to predict fatigue life in case of overload induced retardation / variable amplitude loading, which are divided into three main categories: the yield zone models [14–16], crack closure models [17–21] and strip yield models [22,23]. In addition to those there are other retardation models [24–26] based on damage accumulation and the strain energy release rate, but each model has its own capabilities and limitations as discussed in several literature [27,28]. Because of the complexity, large ambiguities and disagreements, and also lack of proper understanding of the mechanism of retardation, no

* Corresponding author. Tel.: +91 661 2462518.
E-mail addresses: pkray@nitrkl.ac.in, prabal_kray@yahoo.com (P.K. Ray).

Nomenclature

a	crack length measured from edge of the specimen (mm)
a_i	crack length corresponding to the 'ith' step (mm)
a_j	crack length corresponding to the 'jth' step (mm)
a_f	final crack length (mm)
a_{ol}	crack length at overload (mm)
a_d	retarded crack length (mm)
a_d^P	retarded (predicted) crack length (mm)
a_d^W	retarded (Wheeler) crack length (mm)
a_d^E	retarded (experimental) crack length (mm)
A', B', C' and D'	curve fitting constants in the 'exponential model'
B	plate thickness (mm)
C	constant in the Paris equation
COD	crack opening displacement
$(C_p)_i$	retardation parameter
da/dN	crack growth rate (mm/cycle)
$(da/dN)_{retarded}$	retarded crack growth rate (mm/cycle)
E	modulus of elasticity (MPa)
f(g)	geometrical factor
F	remotely applied load (N)
F_{max}	maximum load of constant amplitude load cycle (N)
$F_{max(ol)}$	maximum load at overload (N)
F_{min}	minimum load of constant amplitude load cycle (N)
K	stress intensity factor (MPa$\sqrt{m}$)
K_C	plane stress fracture toughness (MPa$\sqrt{m}$)
K_{IC}	plane strain fracture toughness (MPa$\sqrt{m}$)
K_{max}	maximum stress intensity factor (MPa$\sqrt{m}$)
K_{max}^B	maximum (base line) stress intensity factor (MPa$\sqrt{m}$)
K_{ol}	stress intensity factor at overload (MPa$\sqrt{m}$)
ΔK	stress intensity factor range (MPa$\sqrt{m}$)
ΔK_{eff}	maximum stress intensity factor (MPa$\sqrt{m}$)
l	dimensionless factor in the 'exponential model' formulation
m	specific growth rate
m_{ij}	specific growth rate corresponding to the interval i–j
n	exponent in the Paris equation
N	number of cycles or fatigue life
N_i	number of cycles corresponding to the 'ith' step
N_j	number of cycles corresponding to the 'jth' step
N_f	final number of cycles
N_d	number of delay cycle
N_d^P	number of delay cycle (predicted)
N_d^W	number of delay cycle (Wheeler)
N_d^E	number of delay cycle (experimental)
N_f^P	final number of cycles (predicted)
N_f^E	final number of cycles (experimental)
p	shaping exponent in the Wheeler model
r_{pi}	current plastic zone size corresponding to the 'ith' cycle (mm)
r_{po}	overload plastic zone size (mm)
R	load ratio
R_{ol}	overload ratio
t	time
w	plate width (mm)
γ	retardation correction factor
λ	plastic zone correction factor
v	Poison's ratio
σ_{ys}	yield point stress (MPa)
σ_{ut}	ultimate stress (MPa)

fundamental and universally accepted model is available that would include all the mechanisms and could be applied to all materials. From engineering point of view, retardation models should be calibrated by experimental data fitting as recommended by Broek [29]. Therefore, for successful implementation of life prediction methodologies to the design and in-service operation of structures subjected to variable amplitude loading (CAL with tensile overload spike), empirical models are under constant improvement.

The prediction of life is a challenging job for the engineering community because of two reasons. Firstly it involves a robust integration scheme; secondly no single universal method is available as far as the different load interaction mechanisms are concerned. The authors have adopted an exponential model for life prediction under constant amplitude loading (Part I of this article). Here the authors have taken one step ahead to predict the retarded fatigue life due to single spike overload by using the same model.

2. Experimental procedure

This study was conducted on 7020-T7 Al-alloy and 2024-T3 Al-alloy. The chemical composition and the mechanical properties of the alloys are given in Tables 1 and 2 respectively. Fatigue crack growth tests were conducted in air at room temperature on a servo-hydraulic dynamic testing machine (*Instron*-8502) having a load capacity of 250 KN with a frequency of 6 Hz under constant amplitude loading. Single-edge notched specimens used in this study were made in the LT plane, with the loading aligned in the longitudinal direction. The detail geometry of the specimens is illustrated in Fig. 1.

Pre-cracking the specimens was done up to an a/w ratio of 0.3 in mode-I loading with a sinusoidal waveform using a stress ratio of 0.1. The crack growth was monitored with the help of a COD gauge mounted on the face of the machined notch. The stress intensity factor K was calculated using equations proposed by Brown and Srawley [30] as follows:

$$K = f(g).\frac{F\sqrt{\pi a}}{wB} \tag{1}$$

$$\text{where, } f(g) = 1.12 - 0.231(a/w) + 10.55(a/w)^2 - 21.72(a/w)^3 + 30.39(a/w)^4 \tag{2}$$

The fatigue crack was allowed to grow up to an a/w ratio of 0.4 and subsequently subjected to single spike overload cycle at a loading rate of 8 kN/min.

The specimens were subjected to mode-I overloads at different overload ratios such as 2, 2.25, 2.35, 2.5, 2.6, and 2.75 for 7020-T7 Al-alloy and 1.5, 1.75, 2.0, 2.1, 2.25 and 2.5 for 2024-T3 Al-alloy. The overload ratio is defined as

$$R_{ol} = \frac{K_{ol}}{K_{max}^B} \tag{3}$$

where, K_{max}^B is the maximum stress intensity factor for base line test. After application of the overload the specimens were subjected to mode-I constant amplitude load cycles.

3. Formulation of the 'exponential model'

3.1. Description of the model

Development of the model has been discussed in Part I (through Eqs. (5)–(13)).

Table 1
Chemical composition of 7020-T7 and 2024-T3 Al-alloys

Matls.	Al	Cu	Mg	Mn	Fe	Si	Zn	Cr	Others
7020-T7 Al-alloy	Main constituent	0.05	1.2	0.43	0.37	0.22	4.6	–	–
2024-T3 Al-alloy	90.7–94.7	3.8–4.9	1.2–1.8	0.3–0.9	0.5	0.5	0.25	0.1	0.15

Table 2
Mechanical properties of 7020-T7 and 2024-T3 Al-alloys

Material	Tensile strength (σ_{ut}) MPa	Yield strength (σ_{ys}) MPa	Young's modulus (E) MPa	Poisson's ratio (ν)	Plane strain fracture toughness (K_{IC}) MPa$\sqrt{m}$	Plane stress fracture toughness (K_C) MPa$\sqrt{m}$	Elongation
7020-T7 Al-alloy	352.14	314.7	70,000	0.33	50.12	236.8	21.54% over 40 mm GL
2024-T3 Al-alloy	469	324	73,100	0.33	37.0	95.31	19% over 12.7 mm GL

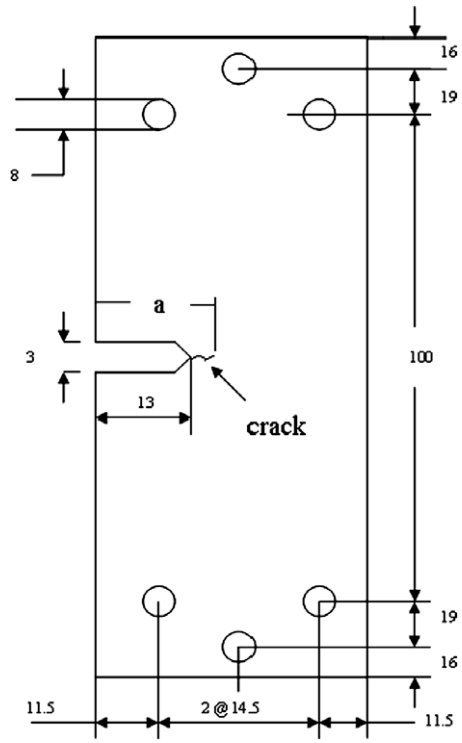

Fig. 1. Single-edge notched specimen geometry.

The exponential equation for crack growth is written as:

$$a_j = a_i e^{m_{ij}(N_j - N_i)} \tag{4}$$

$$m_{ij} = \frac{\ln\left(\frac{a_j}{a_i}\right)}{(N_j - N_i)} \tag{5}$$

where a_i and a_j = crack length in ith step and jth step in 'mm', respectively, N_i and N_j = no. of cycles in ith step and jth step, respectively, m_{ij} = specific growth rate in the interval i–j, i = no. of experimental steps, and $j = i + 1$.

The values of m can be calculated from crack length and number of load cycles data. The a-N curves for various overload conditions are presented in Figs. 2 and 3, respectively for both the materials. The important parameter in the model is the specific growth rate 'm'. This is correlated with two crack driving forces such as K_{max}, and ΔK, as well as the material parameters K_C, E and σ_{ys}, and is defined by the equation

$$m = A'l^3 + B'l^2 + C'l + D' \tag{6}$$

$$\text{where, } l = \left[\left(\frac{\Delta K}{K_C}\right)\left(\frac{K_{max}}{K_C}\right)\left(\frac{\sigma_{ys}}{E}\right)\right]^{\frac{1}{4}} \tag{7}$$

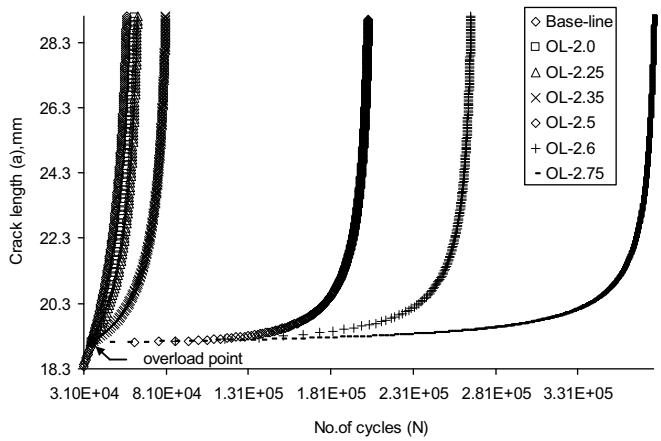

Fig. 2. a-N curve for different overload ratios (7020-T7 alloy).

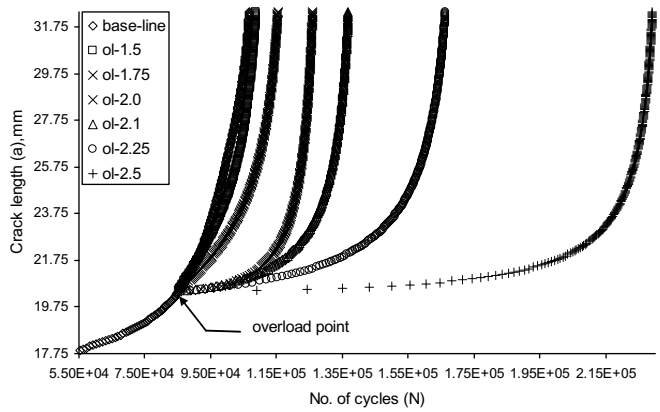

Fig. 3. a-N curve for different overload ratios (2024-T3 alloy).

It may be noted that since the tests have been conducted in plane stress condition, plane stress fracture toughness (K_C) has been used instead of plane strain fracture toughness (K_{IC}). It is calculated from plane strain fracture toughness (K_{IC}) using an empirical relation proposed by Irwin [31] as follows:

$$K_C^2 = K_{IC}^2(1 + 1.4\beta_{IC}^2) \tag{8}$$

$$\text{where, } \beta_{IC} = \frac{1}{B}\left(\frac{K_{IC}}{\sigma_{ys}}\right)^2 \tag{9}$$

The calculated values of plane stress fracture toughness are presented in Table 2. The different 'm' and 'l' values for post-overload region are fitted by a 3rd degree polynomial. The predicted values

of 'm' are obtained from Eq. (6). The values of the constants A', B', C' and D' corresponding to different overloads for the two materials are tabulated in Tables 3 and 4, respectively. Since the values of the above constants are different for each overload ratio, they are again correlated with R_{ol} by a 2nd degree polynomial with regression coefficient (R^2 value) of 0.998 for both the materials. Eqs. (10)–(13) give the correlations for 7020-T7 Al-alloy and Eqs. (14)–(17) give the correlations for 2024-T3 Al-alloy.

$$A' = (45,168 \times 10^{-6})R_{ol}^2 + (-354,083 \times 10^{-6})R_{ol} + (460,905 \times 10^{-6}) \quad (10)$$

$$B' = (-9600.8 \times 10^{-6})R_{ol}^2 + (81,208 \times 10^{-6})R_{ol} + (-107,645 \times 10^{-6}) \quad (11)$$

$$C' = (354.69 \times 10^{-6})R_{ol}^2 + (-4462.5 \times 10^{-6})R_{ol} + (6389.1 \times 10^{-6}) \quad (12)$$

$$D' = (3.6904 \times 10^{-6})R_{ol}^2 + (49.842 \times 10^{-6})R_{ol} + (-90.813 \times 10^{-6}) \quad (13)$$

and

$$A' = (-31,269 \times 10^{-6})R_{ol}^2 + (127,925 \times 10^{-6})R_{ol} + (-143,543 \times 10^{-6}) \quad (14)$$

$$B' = (13,117 \times 10^{-6})R_{ol}^2 + (-53,849 \times 10^{-6})R_{ol} + (60,396 \times 10^{-6}) \quad (15)$$

$$C' = (-1883 \times 10^{-6})R_{ol}^2 + (7761 \times 10^{-6})R_{ol} + (-8506.5 \times 10^{-6}) \quad (16)$$

$$D' = (86.669 \times 10^{-6})R_{ol}^2 + (-359.11 \times 10^{-6})R_{ol} + (385.94 \times 10^{-6}) \quad (17)$$

The predicted values of m for the tested 7020-T7 Al-alloy specimen (R_{ol} = 2.35) and 2024-T3 Al-alloy specimen (R_{ol} = 2.1) are calculated by putting the values of different constants from Eqs. (10)–(17) in Eq. (6) separately for each material. Then the predicted values of N are calculated as per the following equation:

$$N_j = \frac{\ln\left(\frac{a_j}{a_i}\right)}{m_{ij}} + N_i \quad (18)$$

Table 3
Curve fitting constants of 7020-T7 Al-alloy

Overload ratio (R_{ol})	$A' \times 10^{-6}$	$B' \times 10^{-6}$	$C' \times 10^{-6}$	$D' \times 10^{-6}$
2.0	−68,004	16,721	−1149.9	24.582
2.25	−104,212	25,796	−1793.1	38.17
2.5	−136,870	33,690	−2398.5	52.668
2.6	−165,538	41,857	−3113.5	72.101
2.75	−166,698	41,801	−3084.1	70.865

Table 4
Curve fitting constants of 2024-T3 Al-alloy

Overload ratio (R_{ol})	$A' \times 10^{-6}$	$B' \times 10^{-6}$	$C' \times 10^{-6}$	$D' \times 10^{-6}$
1.5	−22,226	9137.4	−1088.2	41.208
1.75	−14,173	6054.7	−709.26	25.827
2.0	−15,258	5987.1	−545.09	12.189
2.25	−11,951	4822.9	−521.37	16.77
2.5	−19,774	8027.2	−896.03	30.197

3.2. Significance of specific crack growth rate (m)

Each and every fatigue crack growth model developed so far attempts to correlate the crack growth information with different crack driving forces and several other parameters so as to predict the residual fatigue life. In the present model this has been done through specific crack growth rate 'm'. Its value depends on several

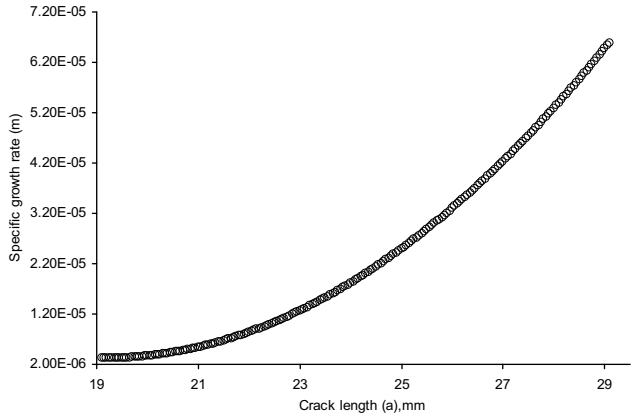

Fig. 4. Variation of specific growth rate with crack length (R_{ol}-2.35, 7020-T7 alloy).

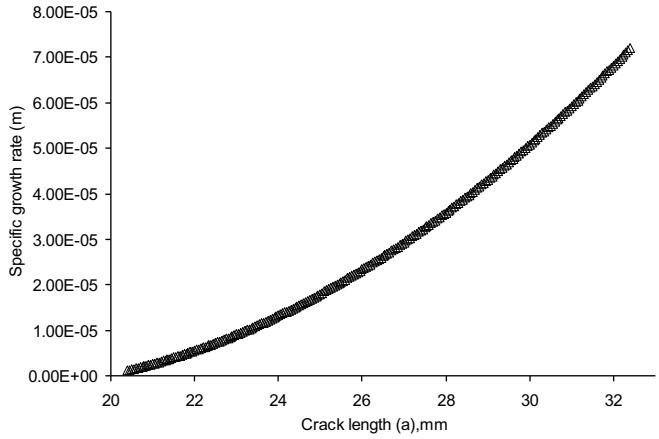

Fig. 5. Variation of specific growth rate with crack length (R_{ol}-2.1, 2024-T3 alloy).

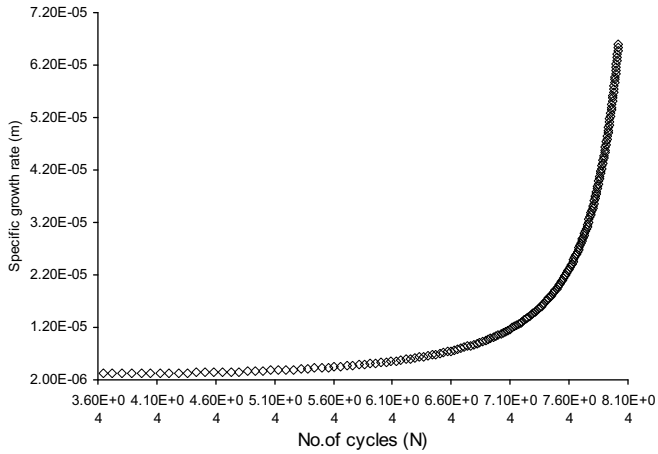

Fig. 6. Variation of specific growth rate with number of cycle (R_{ol}-2.1, 7020-T7 alloy).

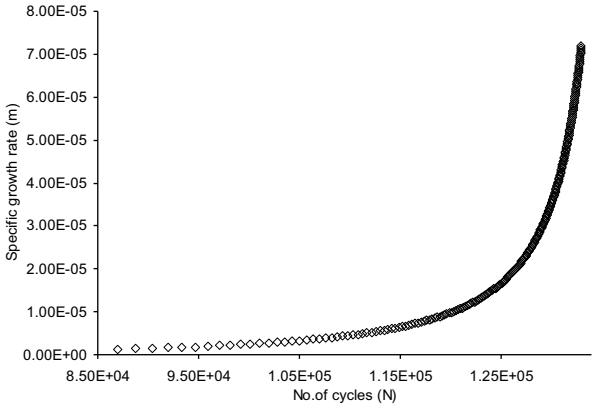

Fig. 7. Variation of specific growth rate with number of cycle (R_{ol}-2.1, 2024-T3 alloy).

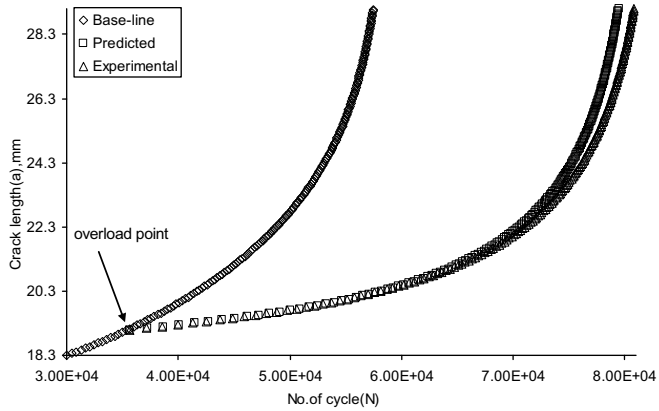

Fig. 8. Comparison of predicted and experimental number of cycle (7020-T7 alloy).

crack driving forces and material properties. According to 'Unified Approach', fatigue crack growth rate not only depends on the single crack driving force ΔK, but also on K_{max} to take into account the mean stress effects [8–13]. Therefore, m will depend on both ΔK and K_{max}. Further, the value of m is also influenced by the plane stress fracture toughness (K_C) of the material, the two material parameters E and σ_{ys} as well as initial crack length. Hence, the dependence of m on these parameters is represented by the dimensionless groups ($\Delta K/K_C$), (K_{max}/K_C), and (E/σ_{ys}), and the relationship is expressed through Eqs. (6) and (7).

It may be noted that m does not remain constant during a test since its value changes with change in loading conditions (ΔK, K_{max}). In a constant load fatigue test, ΔK and K_{max} increase with increase in crack length and also with number of cycles. Hence the specific growth rate m also increases with increase in crack length and number of cycles. The variation of m with crack length and number of cycles are shown in Figs. 4–7 respectively.

4. Validation of the proposed model

The fatigue crack growth data of 7020-T7 and 2024-T3 aluminum alloys (R_{ol} = 2.35 and R_{ol} = 2.1, respectively) were used for the validation of the proposed model. The different retardation parameters were compared with experimental results and also with Wheeler model to verify the accuracy of the model. The load scenarios of the tested specimens are presented in Table 5.

4.1. Comparison with experimental results

The present model has been tested by comparing experimental data with the predicted results for overload ratio of 2.35 (R_{ol} = 2.35) for 7020-T7 and 2.1 (R_{ol} = 2.1) for 2024-T3 specimens. Figs. 8 and 9 show the experimental and predicted a-N curve for the tested specimens. The experimental and the predicted values of retarded crack length and delay cycle for both the cases have been presented in Table 6. Figs. 10 and 11 show that the predicted da/dN-ΔK plots do match with the experimental curves for the tested overload ratios in both the alloys.

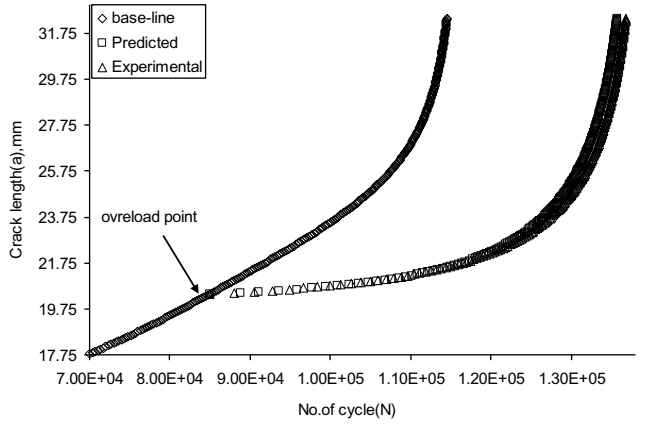

Fig. 9. Comparison of predicted and experimental number of cycle (2024-T3 alloy).

4.2. Comparison with 'Wheeler model'

For determination of the various retardation parameters such as retarded crack length (a_d) and delay cycles (N_d), it is necessary to calculate the shaping exponent in Wheeler model. The Wheeler model parameters are shown in Fig. 12. The Wheeler retardation relation for the delay in crack growth due to a single tensile overload is given by:

$$\left(\frac{da}{dN}\right)_{\text{retarded}} = (C_p)_i[C(\Delta K)^n] \tag{19}$$

where, $(C_p)_i$ is the retardation parameter and is given by

$$(C_p)_i = \left(\frac{r_{pi}}{[a_{ol} + r_{p0} - a_i]}\right)^p \tag{20}$$

where, p = empirically determined shaping parameter, a_{ol} = crack length at overload, and r_{p0} = overload plastic zone size, that can be calculated, assuming plane stress loading using the following expression:

Table 5
Load scenarios of the tested specimens

Test sample	F_{max} (KN)	F_{min} (KN)	$F_{max(ol)}$ (KN)	R_{ol}	a_i (mm)	a_{ol} (mm)	a_f (mm)
7020-T7	7.856	0.7856	18.462	2.35	18.30	19.10	29.10
2024-T3	7.305	0.7305	15.341	2.10	17.75	20.40	32.40

Table 6
Experimental results of the tested specimens

Test sample	a_d^Pmm	a_d^Wmm	a_d^Emm	%error in a_d^P	%error in a_d^W	$N_d^P\times10^3$ cycle	$N_d^W\times10^3$ cycle	$N_d^E\times10^3$ cycle	%error in N_d^P	%error in N_d^W	$N_f^P\times10^3$ cycle	$N_f^E\times10^3$ cycle	%error in N_f^P
7020-T7	2.10	2.20	2.13	−1.4	+3.286	29.89	29.80	30.5	−2.03	−2.32	79.46	80.82	−1.68
2024-T3	2.06	2.45	2.18	−5.5	+12.39	36.65	34.52	37.6	−2.53	−8.19	135.75	136.80	−0.77

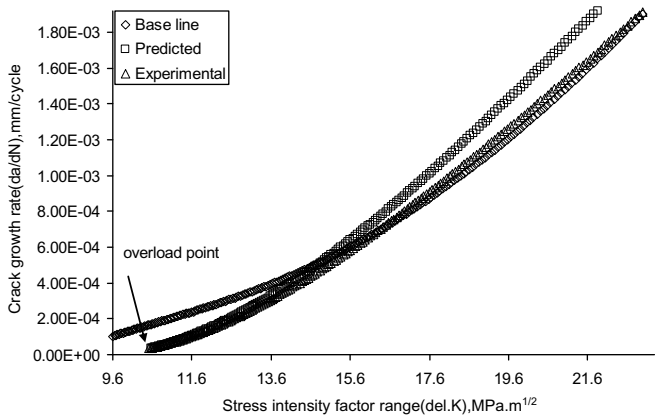

Fig. 10. Comparison of predicted and experimental crack growth rate (7020-T7 alloy).

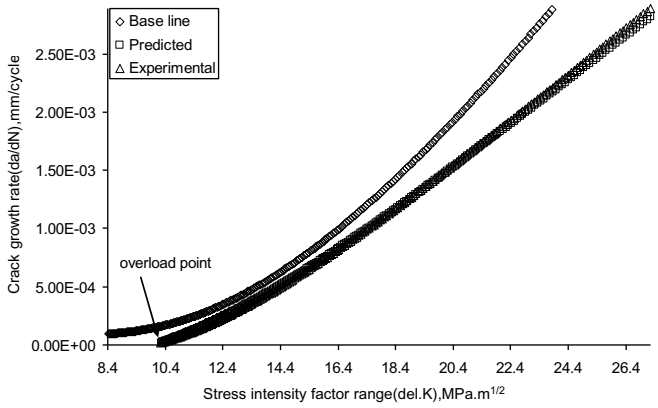

Fig. 11. Comparison of predicted and experimental crack growth rate (2024-T3 alloy).

$$r_{po}=\frac{1}{\pi}\left(\frac{K_{ol}}{\sigma_{ys}}\right)^2 \tag{21}$$

Assuming plane stress loading conditions, the current cyclic plastic zone r_{pi} can be calculated from the expression given below:

$$r_{pi}=\frac{1}{\pi}\left(\frac{\Delta K}{2\sigma_{ys}}\right)^2 \tag{22}$$

The presence of a net compressive residual stress field around the crack tip reduces the usual size of the plane stress cyclic plastic zone size. Therefore, Ray et al. [32] introduced a plastic zone correction factor λ in the expression of the instantaneous cyclic plane stress plastic zone size in a compressive stress field.

$$r_{pi}=\lambda\left(\frac{1}{\pi}\right)\left(\frac{\Delta K}{2\sigma_{ys}}\right)^2 \tag{23}$$

Eq. (20) is now written as

$$(C_p)_i=\left(\frac{\lambda r_{pi}}{[a_{ol}+r_{po}-a_i]}\right)^p=\gamma\left[\frac{r_{pi}}{(a_{ol}+r_{po}-a_i)}\right]^p \tag{24}$$

where, γ is a correction factor which is expressed as $\gamma=\lambda^p$.

The values of γ, λ and p calculated using Eqs. (19) and (24) are presented in Table 7 for both the materials. Using these values, the crack lengths and the corresponding number of cycles have been calculated. The resulting *a-N* curves are presented in Figs. 13 and 14 while d*a*/d*N*-Δ*K* curves are presented in Figs. 15 and 16 along with experimental data and present exponential model for comparison. The different calculated retardation parameters have been

Table 7
Values of material parameters used in Paris and Wheeler model for the tested specimens

Test sample	C	n	λ	p	γ
7020-T7	6×10^{-8}	3.14763	3.5931	0.4246	1.7213
2024-T3	6×10^{-8}	3.270	0.7385	0.3748	0.8926

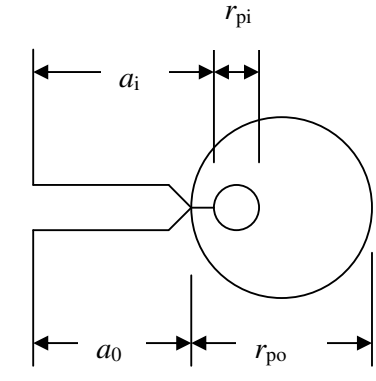

Fig. 12. Plastic zone size definitions used in Wheeler's model.

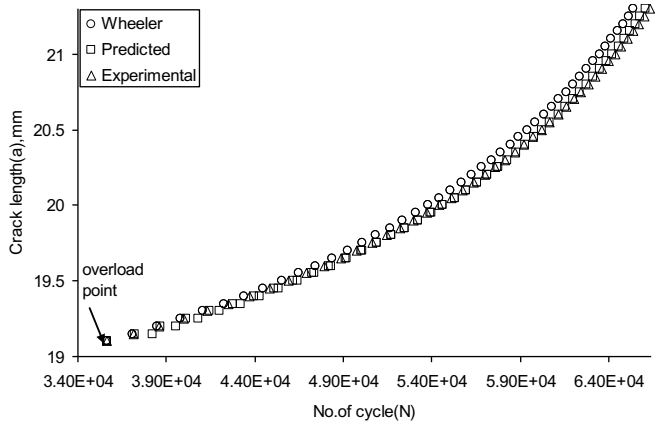

Fig. 13. Comparison of Wheeler, predicted and experimental number of cycle (7020-T7 alloy).

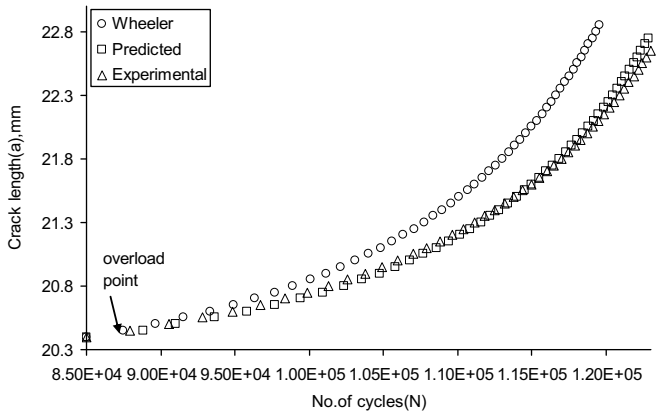

Fig. 14. Comparison of Wheeler, predicted and experimental number of cycle (2024-T3 alloy).

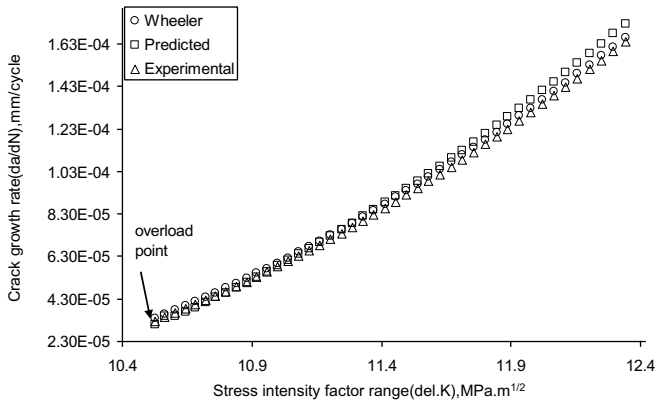

Fig. 15. Comparison of Wheeler, predicted and experimental crack growth rate (7020-T7 alloy).

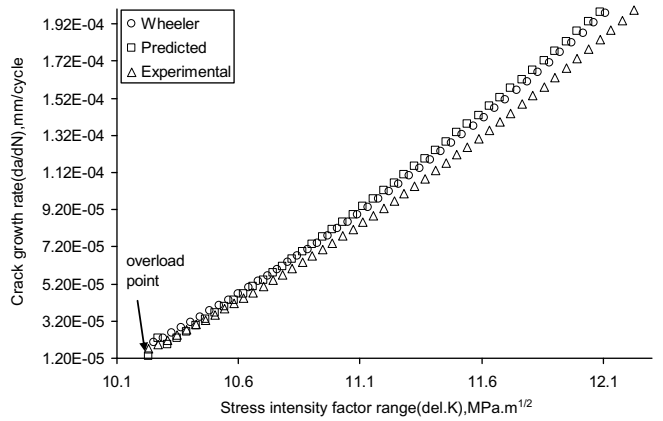

Fig. 16. Comparison of Wheeler, predicted and experimental crack growth rate (2024-T3 alloy).

given in Table 6 for the quantitative comparison of the predicted results.

5. Summary and conclusion

An 'exponential model' has been proposed for the prediction of crack growth behavior and various retardation parameters in case of single overload spike induced constant amplitude loading condition. The predicted results are compared with the experimental data and the values obtained from Wheeler's retardation model. Since interactions between plastic zones are non-linear and also significant ambiguity and disagreements still exist in terms of the exact mechanism of retardation due to overloads, some general rules should be approximated in the quantification of the transient effects and hence in life prediction [27]. Although the present model, in its current form, does not invoke any dominant physical mechanisms leading to retardation of propagating fatigue cracks, but its validation comparisons confirm that the model's accuracy is satisfactory.

The following are concluded from the above discussions:

1. Exponential model of the form $a_j = a_i e^{m_{ij}(N_j - N_i)}$ can be effectively used to determine the retardation parameters 'a_d' and 'N_d' as well as residual fatigue life with reasonable accuracy.
2. The value of m increases with crack extension and number of cycles.
3. In the retardation zone the intrinsic growth rate 'm' is a function of loading parameters defined by ΔK and K_{max}, the material parameters K_C, E and σ_{ys}, the overload ratios (R_{ol}) as well as initial crack length.
4. The intrinsic growth rate m can be represented by an equation of the form $m = A'l^3 + B'l^2 + C'l + D'$ where, $l = [(\frac{\Delta K}{K_C})(\frac{K_{max}}{K_C})(\frac{\sigma_{ys}}{E})]^{\frac{1}{4}}$ and A', B', C' and D' are functions of overload ratios (R_{ol}).
5. Percent errors for the retardation parameters and the cyclic fatigue life predicted by the above model are within reasonable accuracy in comparison to both experimental results and Wheeler's model.

Acknowledgements

The authors wish to record their thanks to CSIR, India for sponsoring this project (project No. 22(373)/04/EMR II). They also thank Hindalco, Renukoot, India for supplying the 7020 aluminum alloy for this research project.

References

[1] Reid LF. Airframe life extension through cold expansion techniques. In: International Conference on Aircraft damage assessment and repair, Melbourne; 1991. p. 109–14.
[2] Lai MO, Nee AYC, Oh JT. Effect of residual stress on the fatigue performance of the structure of a ballised hole. J Mater Process Technol 1992;29:301–9.
[3] Schijive J. Fatigue crack propagation in light alloy steel material and structures. In: Advances in aeronautical sciences. New York: Pergamon Press; 1961. p. 387–408.
[4] Kumar R. A review on crack closure for single overload. Eng Fract Mech 1992;42(1):151–8.
[5] Verma BB, Pandey RK, Chinnadurai R. Effect of loading parameters on post-overload fatigue crack closure. J Test Evaluat 1998;26(6):602–8.
[6] Ranganathan N, Petit J, Fougnet JD. On the influence of the initial ~K level on the post-overload crack propagation behaviour. Adv Fract Res 1984;3:1767–74.
[7] Sadananda K, Vasudevan AK. Analysis of fatigue crack closure and threshold. In: Erdogan F, editor. Fracture mechanics, vol. 25, ASTM STP; 1993. p. 484–501.
[8] Donald K, Paris PC. An evaluation of ΔK_{eff} estimation procedures on 6060-T6 and 2024-T3 aluminum alloys. Int J Fatigue 1999;21:S47–57.
[9] Kujawski D. A new $(\Delta K^+ K_{max})^{0.5}$driving force parameter for crack growth in aluminum alloys. Int J Fatigue 2001;23(8):733–40.
[10] Kujawski D. A fatigue crack driving force parameter with load ratio effects. Int J Fatigue 2001;23:S239–46.
[11] Vasudevan AK, Sadananda K, Louat N. A review of crack closure, fatigue crack threshold and related phenomena. Mater Sci Eng A 1994;188(1–2):1–22.
[12] Dinda S, Kujawski D. Corelation and prediction of fatigue crack growth for different R-ratios using K_{max} and ΔK^+ parameters. Eng Fract Mech 2004;71(12):1779–90.
[13] Noroozi AH, Glinka G, Lambert S. A two parameter driving force for fatigue crack growth analysis. Int J Fatigue 2005;27:1277–96.
[14] Willenborg JD, Engle RM, Wood HA. A crack growth retardation model using an effective stress concept. AFFDL, TM-71-1- FBR. OH: Air Force Flight Dynamics Laboratory, Wright Patterson Airforce Base; 1971.
[15] NASA. Fatigue crack growth computer program. "NASGRO", version 3.0 – reference manual; 2000.

[16] Wheeler OE. Spectrum loading and crack growth. J Basic Eng Trans ASME, Ser D 1972;94(1):181–6.
[17] Elber W. The significance of fatigue crack closure in fatigue. ASTM STP 1972;486:230–42.
[18] Aliaga D, Davy A, Schaff H. Mechanics of fatigue crack closure. In: Newman JC Jr., editor; 1987; p. 491–504.
[19] Padmadinata UH. Investigation of crack-closure prediction models for fatigue in aluminium alloy sheet under flight-simulation loading. PhD-thesis, Delft; 1990.
[20] Baudin G, Labourdette R, Robert M. In: Petit J et al., editors. Fatigue crack growth under variable amplitude loading. London: Elsevier Applied Science; 1988. p. 292–308.
[21] de Koning AU. A Simple crack closure model for prediction of fatigue crack growth rates under variable-amplitude loading. ASTM STP 1981;743:63–85.
[22] Newman Jr JC. A crack-closure model for predicting fatigue crack growth under aircraft spectrum loading. ASTM STP 1981;748:53–84.
[23] de Koning AU, van der Linden HH. Prediction of fatigue crack growth rates under variable loading using a simple crack closure model. NLR MP 81023U, Amsterdam; 1981.
[24] Pompetzki MA, Topper TH, Duquesnay DL, Yu MT. Effect of compressive and tensile overloads on fatigue damage accumulation in 2024-T351 aluminum. J Test Evaluat 1990;18(1):53–61.
[25] Bolotin VV, Lebedev VL. Analytical model of fatigue crack growth retardation due to overloading. Int J Solids Struct 1996;33(9):1229–42.
[26] Lee BL, Kim KS, Nam KM. Fatigue analysis under variable amplitude loading using an energy parameter. Int J Fatigue 2003;25:621–31.
[27] Sadananda K, Vasudevan AK, Holtz RL, Lee EU. Analysis of overload effects and related phenomenon. Int J Fatigue 1999;21:S233–46.
[28] Murthy ARC, Palani GS, Iyer NR. State-of-the-art review on fatigue crack growth analysis under variable amplitude loading. IE (I) J-CV 2004;85: 118–29.
[29] Broek D. The practical use of fracture mechanics. Kluwer; 1988.
[30] Brown WF, Srawley JE. Plane strain crack toughness testing of high strength metallic materials. ASTM STP, ASTM, Philadelphia, USA, vol. 410. 1966. p. 1.
[31] Irwin GR. NRL Report 6598; November 21, 1967.
[32] Ray PK, Ray PK, Verma BB. A study on spot heating induced fatigue crack growth retardation. Fat Fract Eng Mat Struct 2005;28:579–85.